Osteoarthritis and Cartilage Open 8 (2026) 100884

Contents lists available at ScienceDirect

Osteoarthritis and Cartilage Open

journal homepage: www.elsevier.com/journals/osteoarthritis-and-cartilage-open/2665-9131

Inhibition of BMP–Smad1/5 signaling with DMH1 attenuates joint degeneration in a rat model of cuff tear arthropathy

Tomohiro Iuchi [a,b], Kento Shimanoe [b], Takayuki Ide [b,c], Seiya Takada [b], Suguru Saho [a,b], Kohei Uekama [b,d], Yusuke Masuda [b], Hiroki Tawaratsumida [b], Toshiro Ijuin [b], Hiroyuki Tominaga [b], Shingo Maeda [d,*], Noboru Taniguchi [a,b,c,d]

[a] Department of Medical Joint Materials, Graduate School of Medical and Dental Sciences, Kagoshima University, Kagoshima, Kagoshima, 890-8520, Japan
[b] Department of Orthopaedic Surgery, Graduate School of Medical and Dental Sciences, Kagoshima University, Kagoshima, Kagoshima, 890-8520, Japan
[c] Department of Locomotory Organ Regeneration, Graduate School of Medical and Dental Sciences, Kagoshima University, Kagoshima, Kagoshima, 890-8520, Japan
[d] Department of Bone and Joint Medicine, Graduate School of Medical and Dental Sciences, Kagoshima University, Kagoshima, Kagoshima, 890-8520, Japan

ARTICLE INFO

Handling Editor: Professor H Madry

Keywords:
Cuff tear arthropathy
Bone morphogenetic protein
DMH1
Osteoarthritis
Subchondral bone

ABSTRACT

Objective: To characterize bone morphogenetic protein (BMP) signaling in cuff tear arthropathy (CTA) using a modified rat model (mCTA) and determine whether inhibition of DMH1-sensitive BMP type I receptor signaling attenuates CTA pathology.

Design: The rat mCTA model was generated by resection of the supraspinatus and infraspinatus tendons, the superior joint capsule, and the long head of the biceps tendon. Single-cell RNA sequencing (scRNA-seq) was performed to characterize BMP ligand expression in the humeral head. BMP-2, BMP-7, and phosphorylated Smad1/5 (*p*-Smad1/5) were evaluated by immunohistochemistry, and *Id1* expression was assessed by RT-qPCR. Synovial macrophage subsets were assessed by immunostaining. Rats received daily intraperitoneal DMH1 (10 mg/kg) or vehicle for 4 weeks. Histological scores, bone volume, osteoclast number, inflammatory cytokines, catabolic enzymes, and macrophage markers were quantified.

Results: scRNA-seq revealed expression of BMP ligands. In mCTA cartilage, BMP-2 and BMP-7 expression, *p*-Smad1/5 signaling, and hypertrophic markers (Runx2, Col10a1) were upregulated. DMH1 suppressed Smad1/5 activation, reduced inflammatory and catabolic gene expression, and attenuated cartilage degeneration. In subchondral bone, BMP signaling was associated with increased osteoclast numbers, RANKL/OPG imbalance, and reduced bone volume, all of which were improved by DMH1 treatment. In the synovium, BMP signaling and inflammatory mediators were elevated with increased macrophage numbers; DMH1 reduced inflammatory mediators and M1 macrophage numbers.

Conclusions: BMP–Smad1/5 signaling is activated in multiple joint tissues in mCTA and is associated with cartilage degeneration, subchondral bone resorption, and synovial inflammation. These findings suggest that BMP–Smad1/5 signaling may contribute to the pathological changes observed in mCTA.

1. Introduction

Massive rotator cuff tears are frequently associated with lesions of the long head of the biceps brachii (LHB) [1] and superior part of the capsule [2], ultimately leading to cuff tear arthropathy (CTA), a unique form of shoulder osteoarthritis (OA) characterized by progressive deformity of the humeral head accompanied by subchondral bone collapse [3–5]. Unlike the subchondral bone sclerosis typically observed in common forms of OA such as knee OA, subchondral bone collapse is a distinctive pathological feature of CTA [3,6], suggesting that different molecular mechanisms underlie disease progression. However, the signaling pathways responsible for this

* Corresponding author. Department of Bone and Joint Medicine, Graduate School of Medical and Dental Sciences, Kagoshima University, 8-35-1 Sakuragaoka, Kagoshima, Kagoshima, 890-8520, Japan.

E-mail addresses: toushou01.6707@gmail.com (T. Iuchi), shimanoekento@gmail.com (K. Shimanoe), takayuki.ide.3515@gmail.com (T. Ide), k9125830@kadai.jp (S. Takada), suguru.saho@gmail.com (S. Saho), kamabiscus814@gmail.com (K. Uekama), mg70m2000@yahoo.co.jp (Y. Masuda), mamemamex3@yahoo.co.jp (H. Tawaratsumida), iju.iju.1111@icloud.com (T. Ijuin), ygctd828@yahoo.co.jp (H. Tominaga), s-maeda@m3.kufm.kagoshima-u.ac.jp (S. Maeda), tanigu@m2.kufm.kagoshima-u.ac.jp (N. Taniguchi).

https://doi.org/10.1016/j.ocarto.2026.100884
Received 16 March 2026; Accepted 26 September 2026
2665-9131/© 2026 The Author(s). Published by Elsevier Ltd on behalf of Osteoarthritis Research Society International (OARSI). This is an open access article under the CC BY-NC-ND license (http://creativecommons.org/licenses/by-nc-nd/4.0/).

characteristic bone destruction remain poorly understood. We previously developed a modified rat model of CTA (mCTA) by resecting the rotator cuff, the LHB tendon, and the superior half of the joint capsule [7]. This model reproduces the characteristic pathological features of CTA, providing a useful platform for investigating the molecular signaling pathways responsible for CTA-specific subchondral bone collapse.

Bone morphogenetic protein (BMP) signaling is a major regulator of bone remodeling and mechanotransduction [8]. BMPs signal through type I (ALK1, ALK2, ALK3, and ALK6) and type II receptors. Ligand–receptor engagement induces the phosphorylation of Smad1/5, thereby regulating target gene transcription *via* the canonical SMAD pathway [9]. In addition to its essential role in skeletal development, BMP signaling is activated in response to inflammatory cytokines and mechanical stimuli, both of which characterize the pathological microenvironment of CTA [6,7,10]. Tumor necrosis factor-α and interleukin-1β (IL-1β) induce BMP-2 expression in chondrocytes [11,12], whereas compressive loading stimulates BMP-4 expression in osteoblasts [13]. These findings suggest that the inflammatory and abnormal mechanical environments characteristic of CTA may promote BMP signaling within the affected joint.

BMP signaling has also been implicated in osteoclast-mediated bone remodeling. BMP ligands stimulate osteoclast differentiation directly and indirectly by increasing receptor activator of nuclear factor-κB ligand (RANKL) expression in osteoblast-lineage cells, thereby promoting bone resorption [14–16]. Unlike conventional knee OA, CTA is characterized by excessive osteoclastogenesis, persistent subchondral bone loss, and progressive subchondral bone collapse rather than the development of subchondral sclerosis [3,6,17]. Although BMP signaling has been extensively studied in knee OA, where it contributes to cartilage degeneration, chondrocyte hypertrophy, and osteophyte formation [18–20], it remains unknown whether BMP signaling regulates the unique osteochondral phenotype of CTA, particularly the persistent imbalance between bone resorption and formation that leads to humeral head collapse. Therefore, this study was designed not simply to determine whether BMP signaling is activated in CTA, but to investigate whether BMP–Smad1/5 signaling contributes to the characteristic pathological features of CTA, including osteoclast-mediated subchondral bone loss and collapse.

In this study, we first characterized the expression and activation of BMP signaling in the modified rat CTA (mCTA) model using single-cell RNA sequencing (scRNA-seq) and immunohistochemical analyses of BMP ligands and phosphorylated Smad1/5 (*p*-Smad1/5). For the loss-of-function experiment, we used dorsomorphin homolog 1 (DMH1), a selective inhibitor of BMP type I receptors that blocks canonical BMP-Smad1/5 signaling while exhibiting greater kinase selectivity than LDN-193189 [21–24]. We hypothesized that aberrant BMP signaling contributes to the excessive osteoclastogenesis and the osteochondral and synovial changes characteristic of CTA and that pharmacological inhibition of this pathway would attenuate disease progression.

2. Methods

All the animal experiments were approved by the Institutional Animal Care and Use Committee of Kagoshima University (approval no. MD24067) and performed according to the Kagoshima University Animal Experimentation Regulations and the ARRIVE guidelines.

2.1. Rat mCTA model

Forty-four 12-week-old male Sprague–Dawley rats were anesthetized with isoflurane. In the right shoulder, the deltoid muscle was incised, and the supraspinatus (SSP) and infraspinatus (ISP) tendons were resected at their insertions onto the humeral head. The superior half of the joint capsule and the LHB tendon were then resected [7]. Sham surgery was performed on the left shoulder through a deltoid incision.

2.2. Single-cell RNA sequencing

For Group 1, both the Sham and mCTA shoulders from two rats (four shoulder samples in total) were analyzed by scRNA-seq 4 weeks after mCTA surgery (Fig. 1A). Cartilage and subchondral bone from the superior to middle humeral head were enzymatically dissociated, labeled with unique hashtag antibodies, pooled, and analyzed using the BD Rhapsody Single-Cell Analysis System. After quality control, 23,214 high-quality cells were obtained from 30,991 initial cells. Candidate cartilage-, bone-, and immune-lineage populations were selected from the full dataset and reclustered as a target subset (2651 cells) for downstream analysis. Detailed procedures for library preparation, preprocessing, quality control, clustering, and reclustering are provided in the Supplementary Information.

2.3. Analysis of mCTA tissues and DMH1 administration

For Group 2, 12 rats were assigned to immunohistochemical analysis or reverse transcription–quantitative polymerase chain reaction (RT-qPCR) analysis (n = 6 animals for each analysis) 4 weeks after surgery (Fig. 2A). For Group 3, 24 rats were randomly assigned to the dimethyl sulfoxide and DMH1 groups (n = 12 animals per treatment group); six animals in each treatment group were used for histological and immunohistochemical analyses, and the remaining six were used for RT-qPCR analysis (Fig. 3A). DMH1 was administered using a protocol based on that reported by Pan et al. for mice [25], using a modified schedule consisting of once-daily intraperitoneal injection at 10 mg/kg beginning on postoperative day 1 and continuing for 4 weeks. The DMH1 dosing solution was prepared as described in the Supplementary Information. The control dimethyl sulfoxide group received daily intraperitoneal injections of an equivalent volume of the vehicle without DMH1. Using this regimen, there was no mortality, and no overt changes in the appearance, behavior, or body weights of the rats were observed (Fig. S1). For Group 4, six rats were assigned to immunohistochemical analysis 3 days after Sham/mCTA surgery (Fig. S4A).

The rats were euthanized by isoflurane overdose, and the shoulder joint tissues were harvested for subsequent analyses.

2.4. Histological examination

The glenohumeral joint and surrounding tissues were isolated, fixed in 10% neutral buffered formalin for 24 h at room temperature, and decalcified in K-CX AT solution (CS-6101; Falma, Tokyo, Japan) at 4 °C for 5 days. Paraffin sections were then prepared and Alcian blue (pH 1.0) staining was performed for the assessment of osteoarthritic changes using the Murine Shoulder Arthritis Score [26].

Regions of interest were predefined anatomically before quantitative analysis. Detailed definitions of the analyzed regions are provided in the Supplementary Information.

2.5. Immunohistochemistry, immunofluorescence and RT-qPCR

Immunohistochemical and immunofluorescence analyses were performed using standard protocols. Details of antigen retrieval, antibodies, staining procedures, and image acquisition are provided in the Supplementary Information. Positive staining was quantified as the proportion of signal-positive cells among total cells. RNA sample preparation and RT-qPCR were performed using standard protocols; detailed procedures are provided in the Supplementary Information.

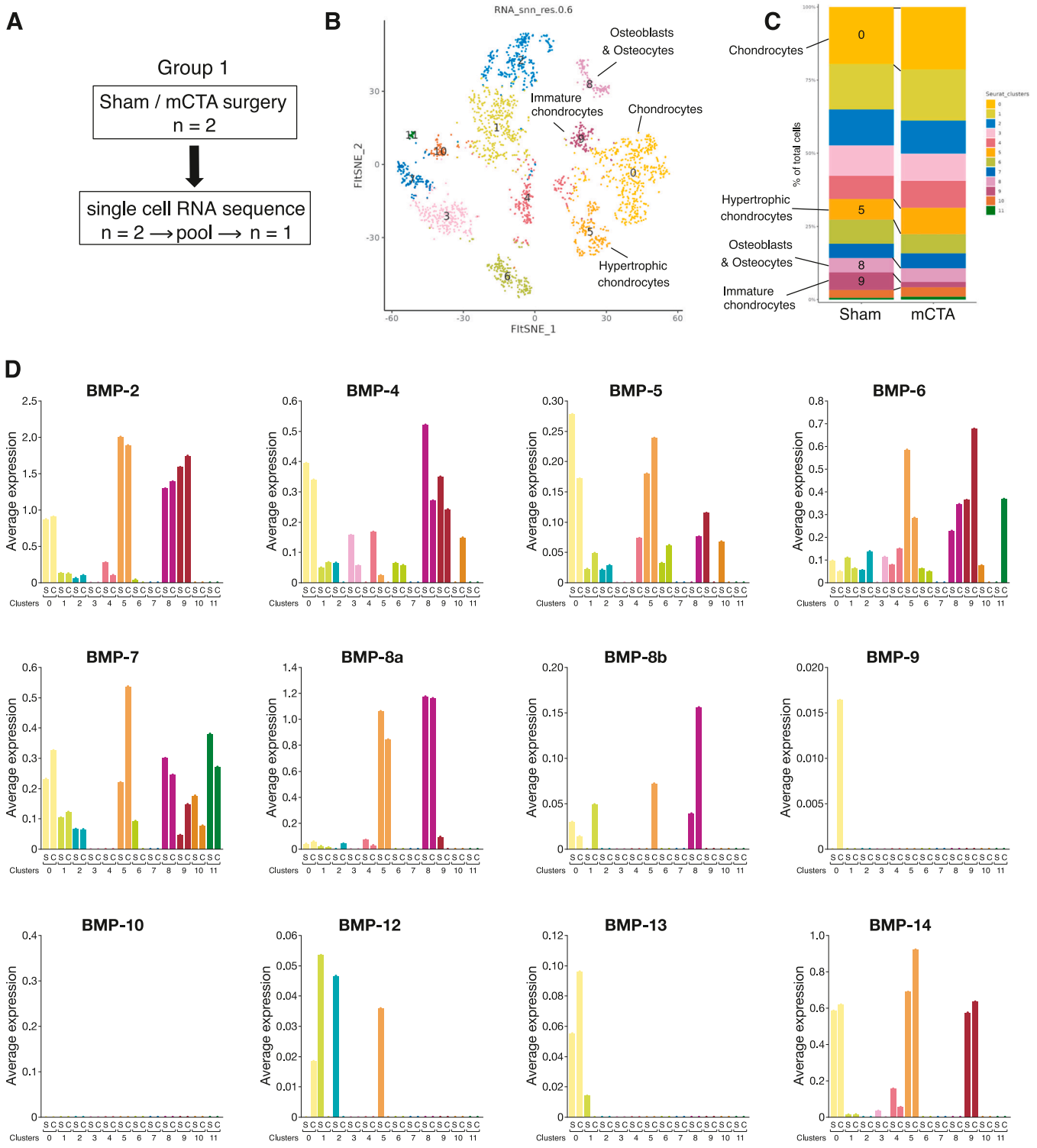


Fig. 1. Results of the single-cell RNA sequencing (scRNA-seq) analysis of the mCTA humeral head and expression of BMP-related genes. (A) Group 1 consisted of two rats; scRNA-seq data were generated from two biological samples per group and pooled for analysis. (B) FIt-SNE plot showing the cell clustering. (C) Proportional distribution of the identified clusters in the Sham and mCTA groups. (D) Expression of BMP genes. S, Sham; C, mCTA.

2.6. Bone volume/tissue volume ratio (BV/TV) and the collapsed area

Hematoxylin and eosin staining of sections was also performed. The BV/TV ratio was then calculated according to the method for murine OA described by Nagira et al. [27]. The humeral head was imaged using the BZ-X710/BZ-X700 microscope system. The subchondral trabecular bone area of the superior zone was defined using BZ-X Analyzer software (Keyence) and measured as the TV and BV. The collapsed area of the humeral head was quantified using a predefined anatomical method described in the Supplementary Information.

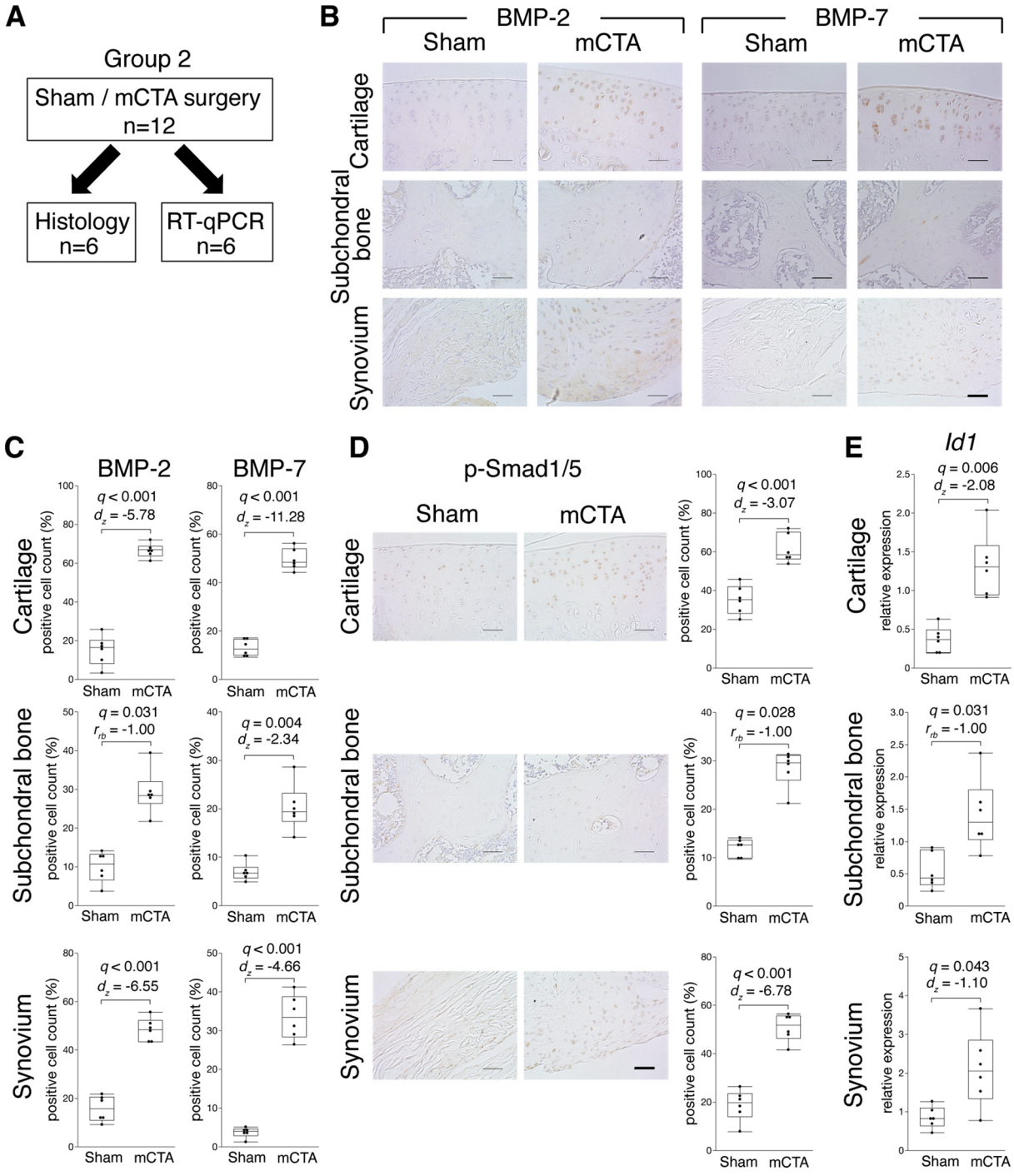


Fig. 2. Expression of BMP-2 and BMP-7 and the activation status of BMP signaling in the articular cartilage, subchondral bone, and synovium of Sham and mCTA rats. (A) Twelve rats in Group 2 were allocated to histological analysis or RT-qPCR analysis. (B) Immunohistochemical staining for BMP-2 and BMP-7 in the articular cartilage, subchondral bone, and synovium. Scale bar = 50 μm. (C) Percentages of the BMP-2- and BMP-7-positive cells shown in (B). (D) Immunohistochemical staining for phosphorylated Smad1/5 (p-Smad1/5) in the articular cartilage, subchondral bone, and synovium (left panels) and the percentages of the cells that were positive (right panels). Scale bar = 50 μm. (E) Relative mRNA expression of *Id1*, assessed using RT-qPCR. n = 6 shoulders in each group.

2.7. Statistical analysis

All histological and image-based quantitative assessments were independently performed by two blinded investigators. The animal was considered the experimental unit, and shoulder-level measurements were used for statistical analyses. Interobserver reliability was assessed using ICC (2,2), demonstrating good-to-excellent agreement across outcomes (range, 0.847–1.000). Detailed statistical procedures and sensitivity analyses are described in the Supplementary Information and Tables.

3. Results

3.1. Exploratory scRNA-seq analysis identifies BMP ligand expression across cartilage and bone cell populations

The target subset used for scRNA-seq analysis comprised 2651 cells, including 1540 cells from the sham group (866 and 674 cells) and 1111 cells from the mCTA group (405 and 706 cells). The scRNA-seq data were subjected to unsupervised clustering and visualized using

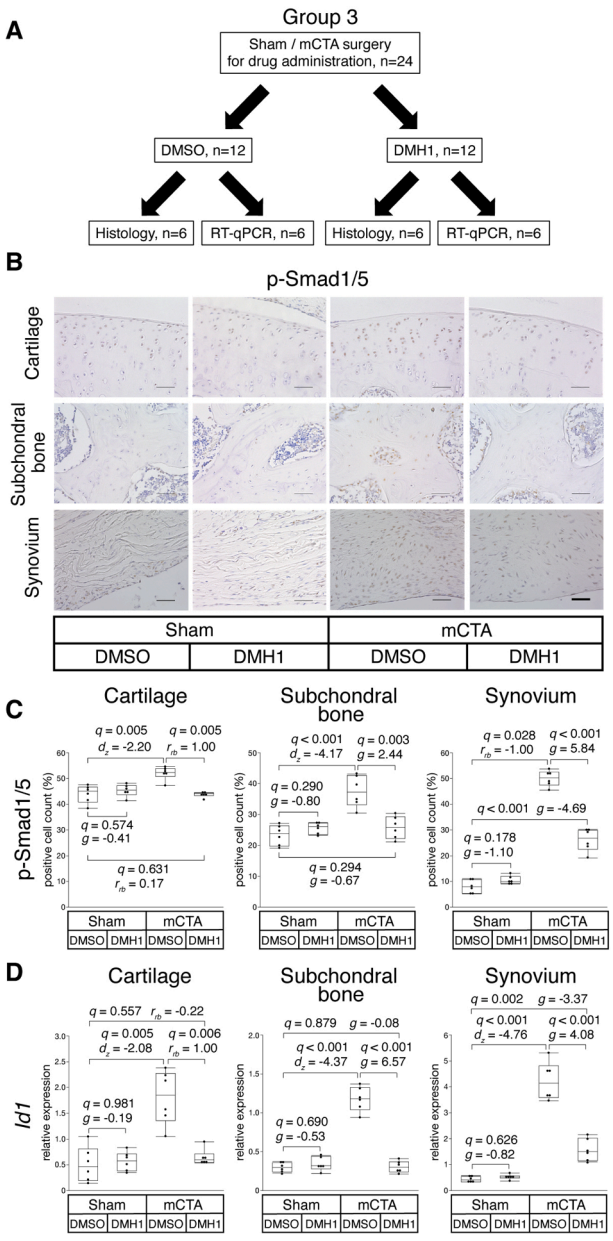


Fig. 3. Effects of DMH1 administration on BMP signaling, assessed using *p*-Smad1/5 and *Id1* expression. (A) The rats in Group 3 were assigned to a control (DMSO-treated) group or a DMH1-treated group, and for each group, tissues from half underwent histological analysis and those from the remaining half underwent RT-qPCR analysis. (B) Immunohistochemical staining for *p*-Smad1/5 in the articular cartilage, subchondral bone, and synovium. Scale bar = 50 μm. (C) Percentages of the *p*-Smad1/5-positive cells shown in (B). (D) Relative mRNA expression of *Id1*, assessed using RT-qPCR. n = 6 shoulders in each group.

FIt-SNE plots. A total of 12 clusters were identified on the FIt-SNE plot (Fig. 1B). By cross-referencing these clusters with FIt-SNE feature plots showing the expression of established markers for chondrocytes, hypertrophic chondrocytes, osteoblasts, and osteocytes (Fig. S2), we identified immature chondrocytes (Cluster 9), chondrocytes (Cluster 0), hypertrophic chondrocytes (Cluster 5), and osteoblasts/osteocytes (Cluster 8) (Fig. 1B). These findings were validated by measuring the expression of cell type-specific marker genes for each cluster (Fig. S3). Because osteoclasts are multinucleated giant cells, they were likely to have been excluded or disrupted during filtering and the other sample preparation procedures, and therefore they were not detected as a cluster in the present scRNA-seq analysis. Analysis of the proportional distribution of each cluster within the total cell population revealed that, in the mCTA samples, the fraction of immature chondrocytes was lower, whereas those of chondrocytes and hypertrophic chondrocytes were slightly higher (Fig. 1C). Immature chondrocytes showed detectable expression of BMP-2, -4, -5, -6, -7, and -14, whereas chondrocytes expressed BMP-2, -4, -5, -7, and -14. Hypertrophic chondrocytes and osteoblasts/osteocytes also expressed multiple BMP ligands, including BMP-2, -5, -6, -7, -8a, and −14 and BMP-2, -4, -5, -6, -7, -8a, and -8b, respectively (Fig. 1D). Comparison between control and mCTA samples demonstrated a tendency toward higher expression of BMP-5, -7, and -14 in hypertrophic chondrocytes and BMP-5, -6, and -8b in osteoblasts/osteocytes in the mCTA group (Fig. 1D). These findings suggested that several BMP ligands were expressed in cell populations potentially involved in CTA pathology, prompting further investigation of BMP signaling activation by immunohistochemical analysis of phosphorylated Smad1/5.

3.2. *BMP-2 and BMP-7 expression and BMP signaling activity in mCTA joints*

We evaluated the expression of BMP-2, a representative member of the BMP-2/4 group that has been reported to be upregulated in knee OA, and BMP-7, a representative of the BMP-5/6/7 subgroup that was found on scRNA-seq to be upregulated in hypertrophic chondrocytes in the mCTA samples (Fig. 1D). For both BMP-2 and BMP-7, immunoreactivity was higher (Fig. 2B) and larger numbers of expressing cells were observed (Fig. 2C) in the articular cartilage, subchondral bone, and synovium in the mCTA model. To assess the activation of the canonical Smad pathway by BMPs, we quantified *p*-Smad1/5-positive cells and found larger numbers in all the tissues evaluated (Fig. 2D). Furthermore, to determine whether increased *p*-Smad1/5 signaling was accompanied by downstream transcriptional activation across all evaluated joint tissues, including the synovium, we measured the mRNA expression of *Id1*, a direct downstream target of BMP signaling [28], by RT-qPCR. *Id1* expression was upregulated in all the evaluated tissues from the mCTA model (Fig. 2E).

3.3. *DMH1-mediated suppression of BMP signaling in mCTA joints*

After 4 weeks of DMH1 treatment (Fig. 3A), *p*-Smad1/5 immunostaining demonstrated near-complete suppression of BMP signaling to control levels in the cartilage and subchondral bone, and approximately 50% suppression in the synovium (Fig. 3B and C). Consistent with this, DMH1 normalized *Id1* expression in the cartilage and subchondral bone, whereas approximately one-third of the increase persisted in the synovium (Fig. 3D). DMH1 administration did not affect the expression of these markers in the Sham shoulders.

3.4. *DMH1 partially attenuates the osteoarthritic changes in the cartilage of mCTA*

Murine Shoulder Arthritis Score assessment showed that DMH1 slightly attenuated the mCTA-induced arthropathic changes (Fig. 4A). Although the expression of the hypertrophic markers Runx2 and Col10a1 had not been measured in the mCTA model, we hypothesized that it would be upregulated, given that they are BMP targets. Both the staining intensity and the number of positive cells were higher in the mCTA joints and were both substantially reduced by DMH1 treatment (Fig. 4B).

As we have previously reported [6,7], the expression of pro-inflammatory cytokines (TNF-α, IL-1β, and IL-6) and catabolic enzymes (MMP-3, MMP-13, and ADAMTS-5) is upregulated in the articular cartilage of mCTA joints, and DMH1 reduced the proportion of expressing cells by approximately 50% (Fig. 4C–F).

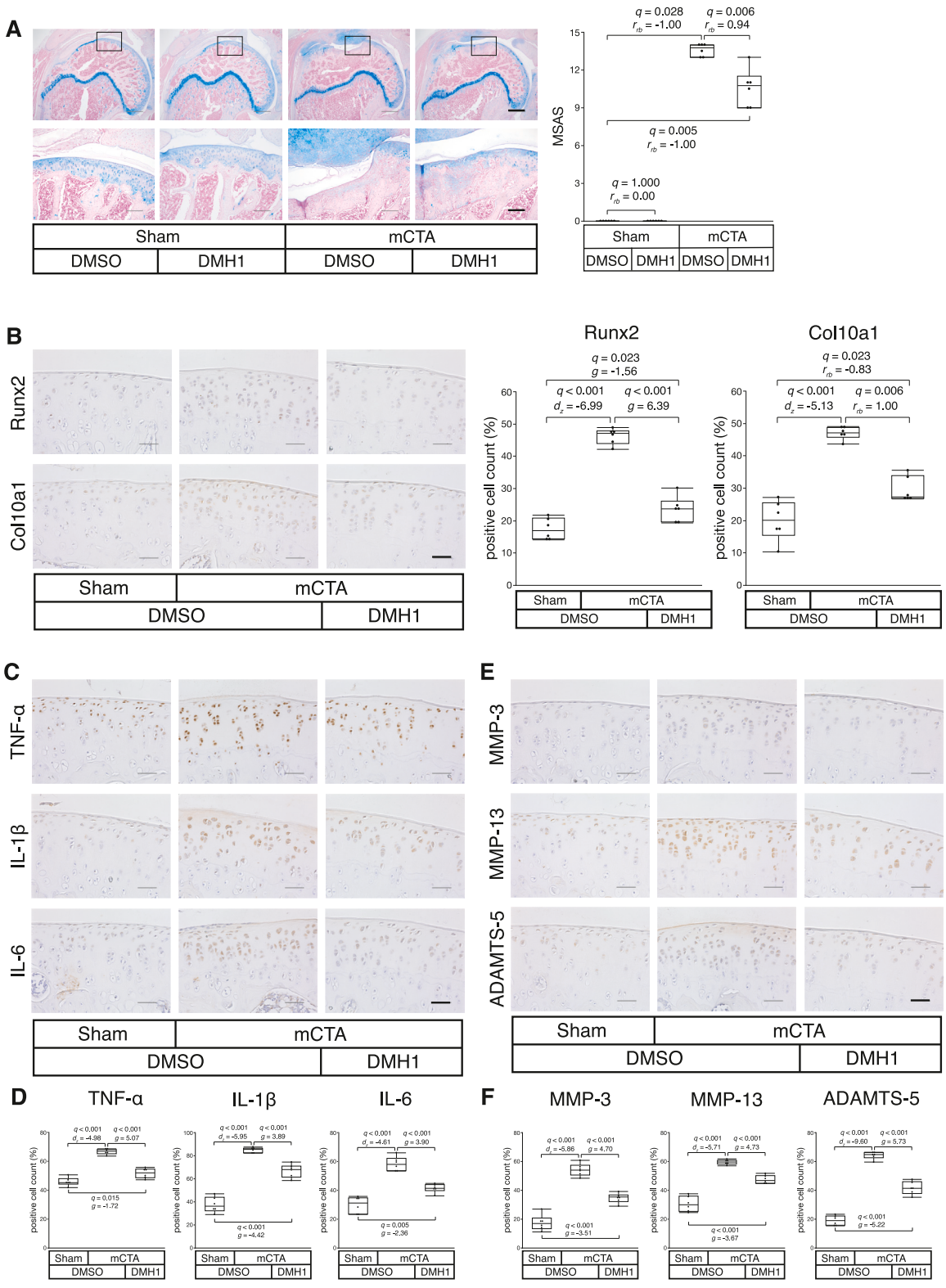


Fig. 4. Effects of DMH1 administration on the MSAS, chondrocyte hypertrophy, and expression of inflammatory cytokines and catabolic enzymes in rats with mCTA. (A) Representative Alcian blue-stained sections (left panels) and the MSAS (right panel). The boxed areas in the upper left images indicate the region shown at higher magnification in the lower panels. Scale bar = 1000 μm (upper panels) and 200 μm (lower panels). (B) Immunohistochemical staining for the hypertrophic chondrocyte markers Runx2 and Col10a1 in the articular cartilage (left panels) and the percentages of the cells that were positive (right panels). Scale bar = 50 μm. (C, D) Immunohistochemical staining for the indicated inflammatory cytokines (C) and the percentages of cells that were positive (D). Scale bar = 50 μm. (E, F) Immunohistochemical staining for the indicated catabolic enzymes (E) and the percentages of the cells that were positive (F). Scale bar = 50 μm. n = 6 shoulders in each group.

3.5. Effects of DMH1 on the subchondral bone of mCTA

DMH1 substantially improved the mCTA-induced reduction in BV/TV, and reduced the collapsed area by ~50% (Fig. 5A). DMH1 administration slightly increased BV/TV in the Sham shoulders. The number of osteoclasts was also reduced by approximately half (Fig. 5B). We also performed immunohistochemical analysis of RANKL, which is essential for osteoclast differentiation, and its antagonist osteoprotegerin (OPG) [29,30]. RANKL expression and the RANKL/OPG ratio, both of which were high in mCTA, were reduced toward the Sham levels by DMH1 (Fig. 5C). Sclerostin is a downstream target of BMP signaling that may mediate these changes

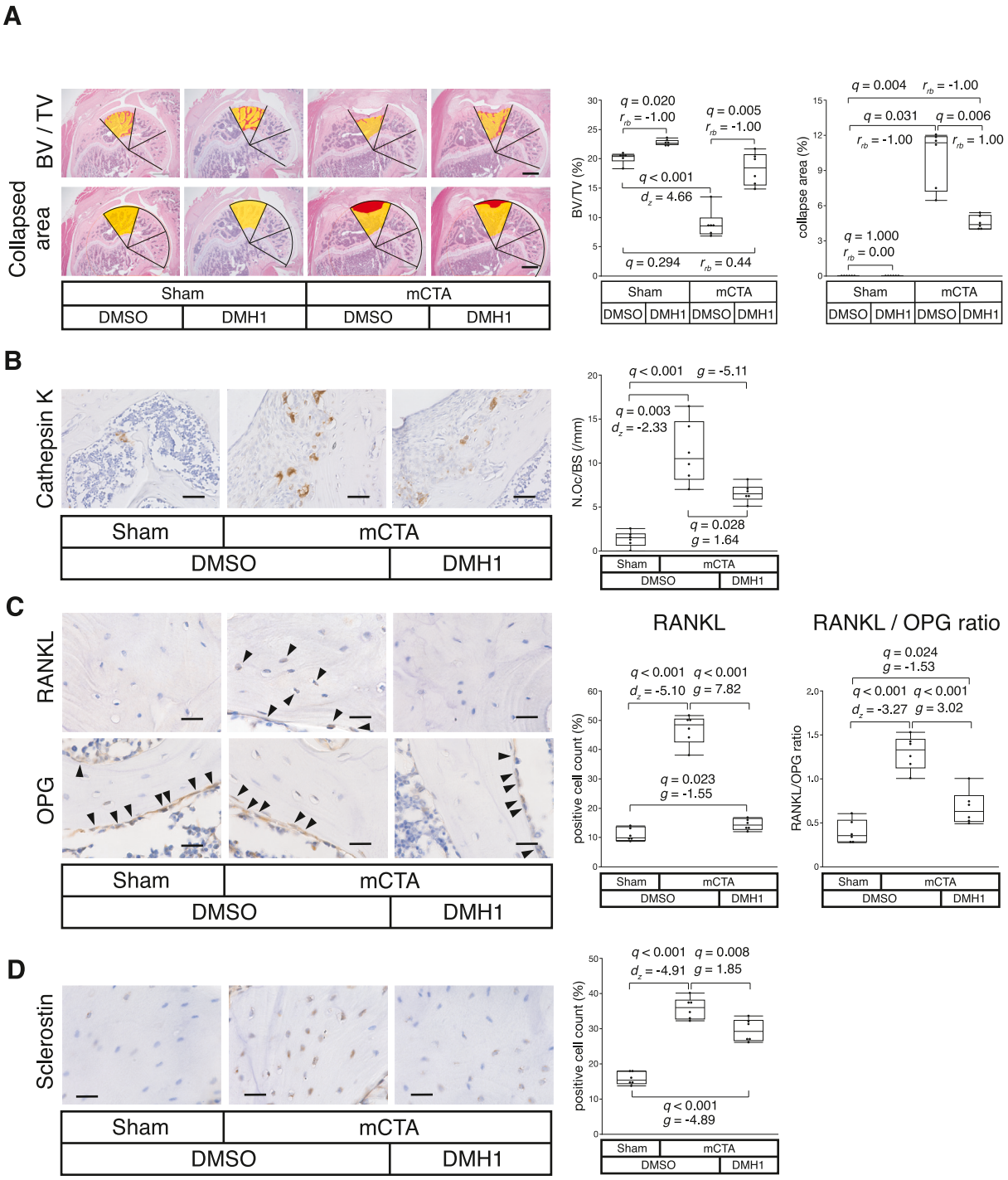


Fig. 5. Effects of DMH1 administration on the subchondral bone volume, collapse, osteoclast number, RANKL/OPG expression ratio, and sclerostin expression in the humeral head of rats with mCTA. (A) Representative hematoxylin and eosin-stained sections (left panels), which were used to measure bone volume/tissue volume (BV/TV) (upper panels; bone volume shown in red and tissue volume in red plus yellow) and the collapsed area ratio (lower panels; superior zone area shown in yellow plus red and collapsed area in red). Scale bar = 1000 μm. The quantification is shown in the right panels. (B) Immunohistochemical staining for cathepsin K to assess the numbers of osteoclasts in the subchondral bone (left panels) and corresponding quantification (right panel). Scale bar = 50 μm. (C) Immunohistochemical staining for RANKL and OPG in the subchondral bone (left panels), and the number of RANKL-positive cells and the ratio of RANKL-to-OPG-positive cells (right panels). Scale bar = 20 μm. Arrowheads indicate positive cells. (D) Immunohistochemical staining for sclerostin in the subchondral bone (left panels) and quantification analysis (right panel) (n = 6). Scale bar = 20 μm. n = 6 shoulders in each group.

in osteoblasts and osteocytes [8], and we found that sclerostin expression was high in mCTA and partially suppressed by DMH1 administration (Fig. 5D).

In the subchondral bone of mCTA, TNF-α expression was reduced by approximately half by DMH1 treatment. In addition, the numbers of IL-1β-, IL-6-, MMP-13-, and ADAMTS-5-positive cells were reduced to levels comparable to those of the Sham group (Fig. 6A–D).

3.6. Effects of DMH1 on the synovium of mCTA

mCTA markedly increased the expression and proportions of cells that were positive for pro-inflammatory cytokines and catabolic enzymes in the synovium, and these increases were approximately halved following DMH1 treatment (Fig. 7A–D). The numbers of synovial M1-like and M2-like macrophages were higher in the mCTA model. DMH1 reduced the numbers of $CD14^+$ monocytes and M1-like macrophages ($iNOS^+$ and $CD80^+$) by approximately half (Fig. 7E and F), whereas its effect on M2-like macrophages ($CD206^+$) was relatively modest.

Finally, to determine whether BMP expression was induced directly by the mCTA procedure or secondarily following the induction of inflammatory cytokines, we examined the temporal relationship between these events by performing immunohistochemical analyses 3 days after mCTA surgery (Fig. S4). At this early time point, neither BMP-2 nor BMP-7 expression was increased in any of the evaluated joint tissues in the mCTA group, and accordingly, no increase in phosphorylated Smad1/5 (*p*-Smad1/5) was observed. In contrast, the expression of TNF-α, IL-1β, and IL-6 was significantly increased in all evaluated tissues.

4. Discussion

The present study extends previous work on BMP signaling in OA by addressing a distinct pathological context, namely CTA, which differs fundamentally from conventional OA by exhibiting persistent osteoclast-mediated subchondral bone loss and collapse rather than compensatory subchondral sclerosis. Our findings suggest that BMP–Smad1/5 signaling is involved not only in cartilage-related OA changes but also in the abnormal bone remodeling process characteristic of CTA. A working hypothesis based on the present findings and previous literature in rats with mCTA is presented in Fig. 8. Several pathways shown in the model are supported by prior literature but were not directly tested in the present study. Surgical disruption of the rotator cuff tendons, superior joint capsule, and LHB tendon alters glenohumeral biomechanics [31,32], resulting in abnormal mechanical stress on the cartilage, subchondral bone, and synovium. Mechanical stress can induce BMP expression and signaling activation in musculoskeletal tissues [33–35]. Such mechanical alterations are likely to trigger the release of damage-associated molecular patterns, including HMGB1 and S100A9, as previously reported in this model [6]. These damage-associated molecular patterns stimulate the production of pro-inflammatory cytokines, including TNF-α, IL-1β, and IL-6, which have been reported to induce BMP expression in musculoskeletal tissues [6,7,10–12]. Consistent with this sequence, our analysis at 3 days after mCTA demonstrated marked increases in pro-inflammatory cytokine expression, whereas BMP-2, BMP-7, and phosphorylated Smad1/5 were not yet increased (Fig. S4). These findings suggest that, in the early phase after mCTA induction, BMP signaling activation is unlikely to precede the inflammatory response and may instead occur downstream of early inflammatory cytokine induction. Previous studies have shown that BMP

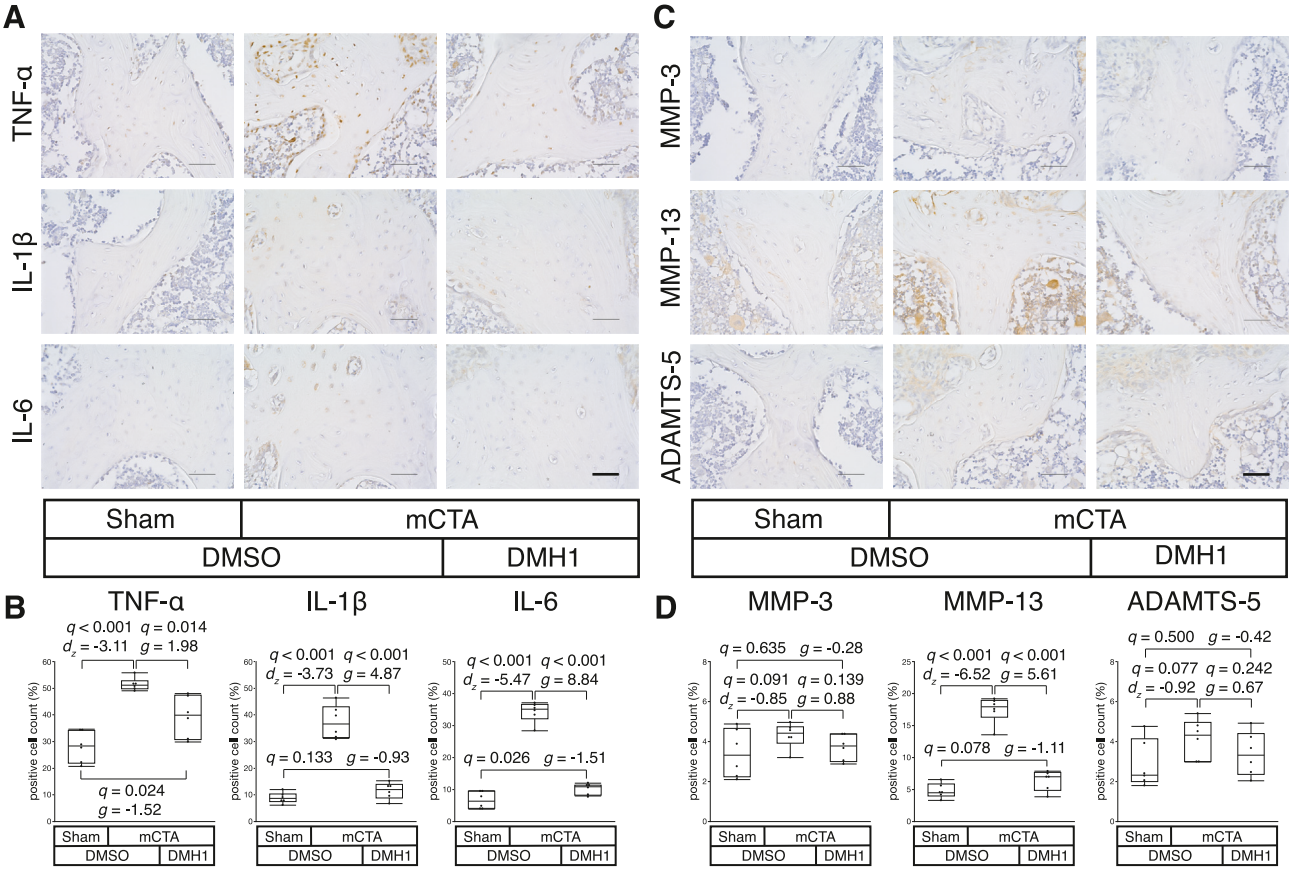


Fig. 6. Effects of DMH1 administration on the expression of inflammatory cytokines and catabolic enzymes in the subchondral bone of rats with mCTA. (A, B) Immunohistochemical staining for the indicated inflammatory cytokines (A) and the percentages of cells that were positive (B). Scale bar = 50 μm. (C, D) Immunohistochemical staining for the indicated catabolic enzymes (C) and the percentages of cells that were positive (D). Scale bar = 50 μm. n = 6 shoulders in each group.

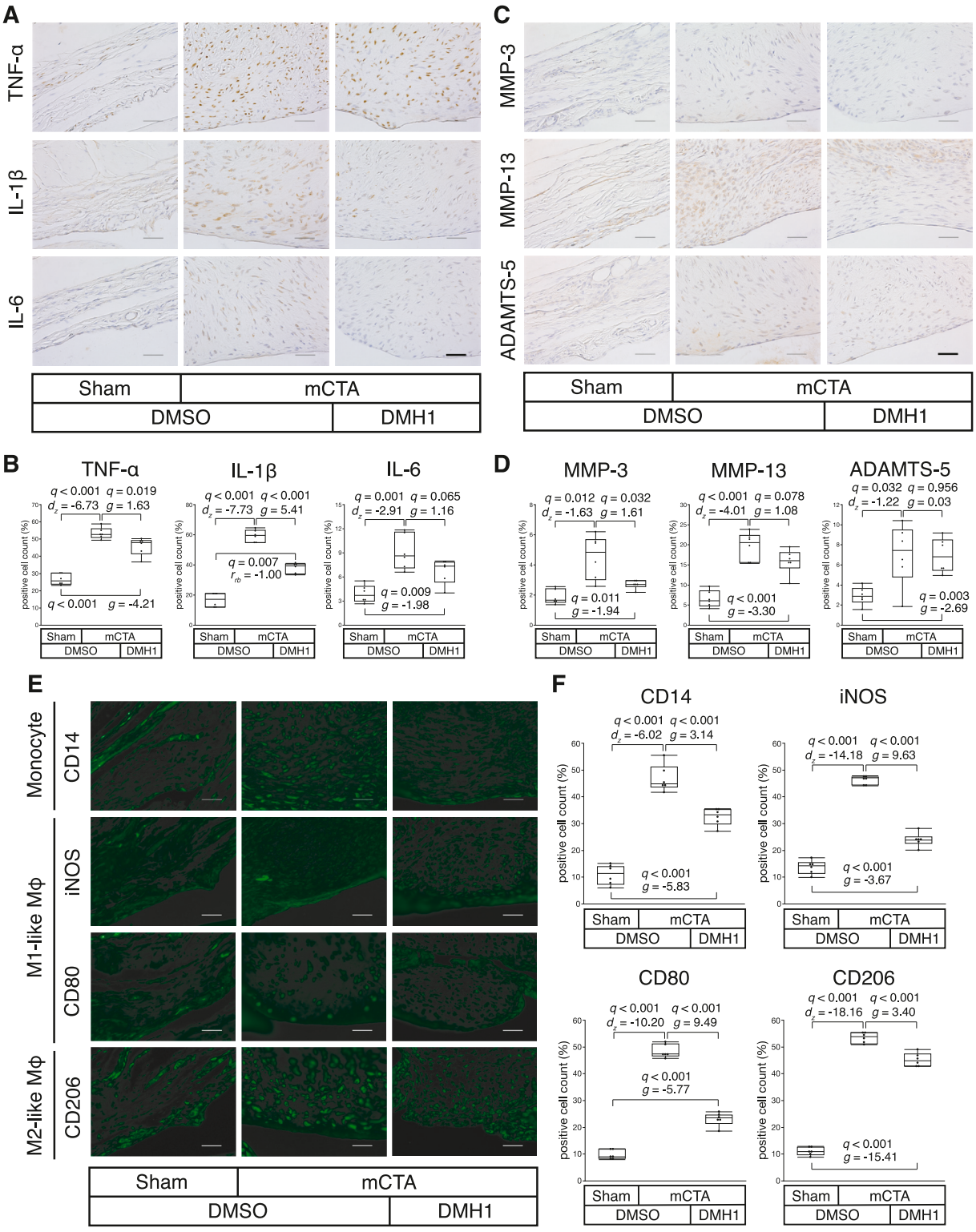


Fig. 7. Effects of DMH1 administration on the synovial inflammation, catabolic enzyme expression, and macrophage polarization of rats with mCTA. (A, B) Immunohistochemical staining for the indicated inflammatory cytokines (A) and the percentages of cells that were positive (B). Scale bar = 50 μm. (C, D) Immunohistochemical staining for the indicated catabolic enzymes (C) and the percentages of cells that were positive (D). Scale bar = 50 μm. (E) Immunofluorescence staining for the indicated markers of monocytes and M1-like and M2-like macrophages (MΦ). Scale bar = 50 μm. (F) Percentages of cells that were positive in (E) (n = 6). n = 6 shoulders in each group.

signaling induces Runx2 expression, thereby promoting chondrocyte hypertrophy through the induction of Col10a1 [36,37]. The present findings are consistent with this mechanism, although a direct causal relationship was not tested in this study.

BMP signaling has been reported to promote osteoclastogenesis both directly and indirectly [15,38] through sclerostin-dependent regulation of the RANKL/OPG axis [8]. The observed changes in sclerostin and RANKL/OPG in the present study are consistent with this mechanism,

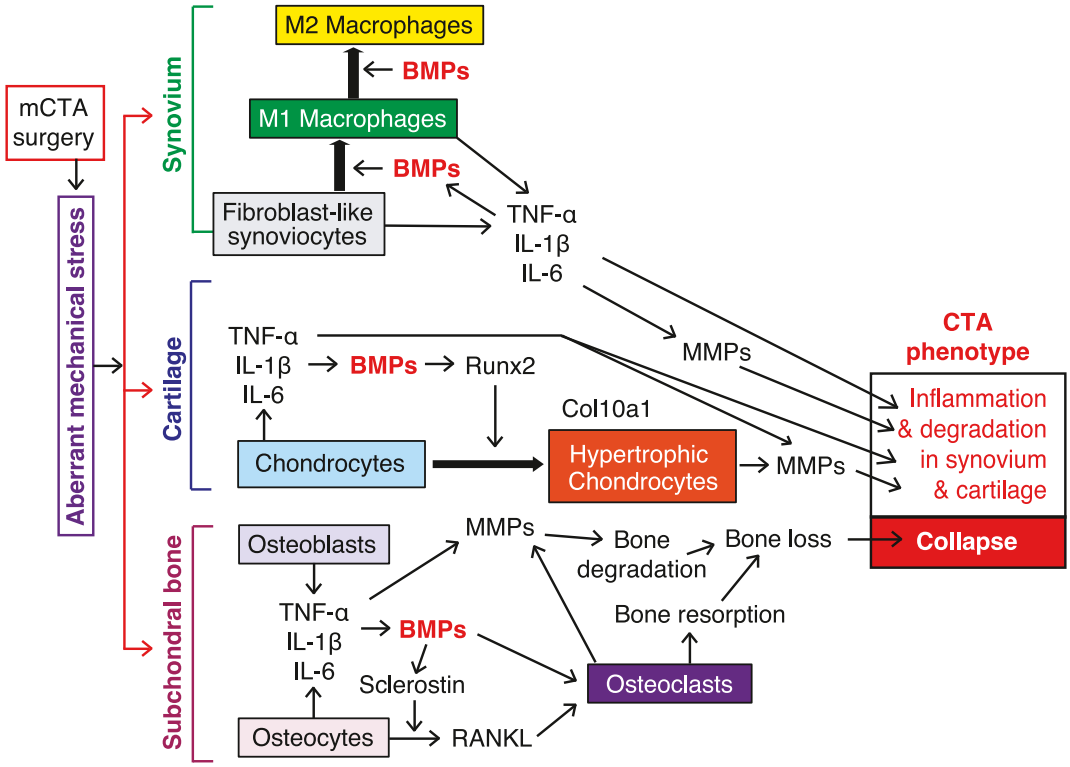


Fig. 8. Working hypothesis summarizing experimentally demonstrated findings and proposed mechanisms inferred from previous studies. Solid findings from the present study are indicated by experimentally supported observations, whereas several mechanistic links are inferred from previous studies and should be considered hypothetical. Resection of the rotator cuff tendons, superior capsule, and long head of the biceps disrupts glenohumeral joint stability, generating abnormal mechanical stress in the articular cartilage, subchondral bone, and synovium. Mechanical stress directly induces DAMPs release and inflammatory cytokine production, which further enhance BMP expression. In cartilage, BMP signaling promotes Runx2-mediated chondrocyte hypertrophy and MMP production, accelerating cartilage degeneration. In subchondral bone, BMPs stimulate osteoclastogenesis directly and indirectly *via* sclerostin induction and an increase in RANKL/OPG ratio, leading to bone resorption and collapse. In the synovium, BMPs and DAMPs promote M1 macrophage polarization and inflammatory cytokine production, but BMP signaling may contribute to M2 polarization, which contributes to both inflammatory regulation and tissue repair.

although direct functional validation was beyond the scope of this work. As a consequence, osteoclast numbers increase, bone resorption is accelerated, and progressive bone loss ultimately results in subchondral bone collapse. In the synovium, BMPs may contribute to M1 macrophage polarization, as suggested by previous studies [39] and by the reduction in M1-like macrophages following DMH1 treatment. However, direct effects on macrophage polarization were not examined in the present study. This shift may cause an increase in the production of pro-inflammatory cytokines, which in turn may further increase BMP expression.

Although several previous genome-wide expression analyses have included BMPs [40,41], there has been no comprehensive survey of the expression of all the BMP family genes in OA cartilage as the primary focus. In the present study, we performed scRNA-seq of articular cartilage and subchondral bone cells from the humeral head of rats with mCTA and analyzed the expression of all the BMP ligands that are capable of activating Smad1/5 signaling (Fig. 1). BMP expression was detected in multiple cell populations, including immature chondrocytes, chondrocytes, hypertrophic chondrocytes, osteoblasts, and osteocytes. Notably, the expression of BMP ligands varied among cell populations. The expression levels of some BMPs were lower, whereas those of others were higher in mCTA samples, suggesting that BMP ligand expression patterns may vary among cell types in the mCTA model. These findings suggest that focusing on individual BMP ligands may be insufficient to understand their biological roles in this model; rather, the integrated activities of the BMP family as a whole should be considered. However, because scRNA-seq was performed using a limited number of animals and the datasets were primarily used for cell-type identification and exploratory characterization of BMP ligand expression patterns, these observations should be considered hypothesis-generating rather than definitive evidence of differential BMP ligand regulation in mCTA. Notably, although immunohistochemistry suggested increased BMP-2 protein expression in mCTA tissues, this observation was not consistently reflected at the transcript level (Fig. 2B and C). Several factors may contribute to such discrepancies, including technical effects associated with tissue dissociation, post-transcriptional regulation, and differences between mRNA and protein turnover. However, these possibilities remain speculative and cannot be confirmed by the present study. In addition, immunohistochemistry is inherently semi-quantitative and may be influenced by antibody specificity, staining conditions, and image-analysis parameters. Therefore, the discrepancy between the transcriptomic and protein-level findings remains unresolved. Future studies employing complementary approaches, such as in situ hybridization (RNAscope), bulk RT-qPCR, or protein-based quantification methods, will be required to validate BMP ligand regulation in the mCTA model.

When considering the effects of DMH1 administration on the mCTA phenotype, it is important to determine whether DMH1 suppresses canonical Smad1/5 signaling. Based on the immunohistochemical assessment of *p*-Smad1/5 and RT-qPCR analysis of *Id1* expression, DMH1 treatment reduced BMP–Smad1/5 signaling in articular cartilage and subchondral bone to levels comparable to those of Sham controls. In contrast, the suppression in the synovium appeared to be incomplete. One possible explanation for this is the differential inhibition of individual type I BMP receptors, which may account for the tissue-dependent effects of DMH1. Therefore, the residual BMP signaling in the synovium may reflect the specific range and relative abundances of the type I BMP receptors expressed in this tissue. Notably, DMH1

administration did not alter *p*-Smad1/5 or *Id1* expression in the Sham shoulders (Fig. 3), suggesting that systemic DMH1 treatment did not substantially suppress physiological levels of BMP signaling under steady-state conditions. However, the slight increase in BV/TV observed in the Sham shoulders after DMH1 administration (Fig. 5A) is consistent with the established role of physiological BMP signaling in regulating bone remodeling and maintaining bone homeostasis [8]. Therefore, it remains possible that DMH1 transiently suppressed BMP signaling even under basal conditions, with the cumulative effects becoming detectable at the tissue level despite the absence of changes in *p*-Smad1/5 or *Id1* expression at the evaluated time point.

There are notable similarities between previously reported findings linking the inhibition of BMP signaling to the attenuation of OA changes, particularly in knee OA models [11,19], and the effects of DMH1 identified in the present mCTA model. Specifically, similar to a study in which the intra-articular administration of the BMP antagonist Noggin ameliorated subchondral bone loss in a rat model of knee OA [11], DMH1 not only attenuated cartilage degeneration but also ameliorated the reduction in subchondral bone mass in the mCTA joints. However, an important distinction between CTA and knee OA lies in the behavior of the subchondral bone. In knee OA, the subchondral bone mass typically decreases during the early phase of the disease, but subsequently progresses to a sclerotic phenotype during the chronic phase [42,43]. In contrast, in CTA, including in advanced disease, subchondral bone loss is maintained, rather than sclerosis developing [6,17]. Clinically, many patients with knee OA present after the disease has already progressed to the chronic phase, by which time subchondral sclerosis has developed [44]. Under such conditions, the therapeutic suppression of BMP signaling in subchondral bone may not provide substantial benefits. In contrast, in CTA, in which subchondral bone loss persists even in severe cases [6,17], targeting BMP signaling may warrant further investigation as a potential therapeutic approach. However, when compared with the previously reported effects of the bisphosphonate zoledronate in the mCTA model [6], the therapeutic effects of DMH1 appear to be relatively mild. This difference may mean that BMP signaling is not a primary driver of the mCTA pathology. Rather, BMP signaling may be one modulator within a more complex network of downstream target genes and interacting pathways (Fig. 8).

Some limitations of the present study should be acknowledged. First, non-canonical BMP pathways, such as p38 MAPK signaling, are not suppressed by DMH1 [24]. Therefore, DMH1 would not fully inhibit all biological effects of BMP ligands. Second, although DMH1 is widely used as a selective inhibitor of BMP type I receptors, its effects cannot be attributed exclusively to BMP ligands, because ALK1 can also be activated by ligands other than BMPs, including TGF-βs. In addition, because DMH1 was administered systemically, the present study cannot distinguish direct effects on articular cartilage, subchondral bone, synovial cells, or immune cells from indirect systemic effects. Therefore, our findings should be interpreted as supporting a contributory role of DMH1-sensitive Smad1/5 signaling in mCTA pathology rather than establishing BMP ligand-specific causality. Third, the use of quadrupeds as a model of CTA represents an inherent limitation. The biomechanics of the rat shoulder differ substantially from those of human shoulders, particularly with respect to overhead activity, range of motion, and loading patterns. However, the use of non-human primates, which are more anatomically comparable to humans, is not realistic from ethical and financial perspectives. Of the commonly available experimental animal species, the rat is considered to have shoulders that are the most anatomically similar to the human shoulder [45]. Therefore, at present, it represents a reasonable and practical model for the investigation of CTA-related pathology. Fourth, we were unable to evaluate the long-term effects of DMH1 during the late phase of disease progression. The intraperitoneal administration of DMH1 is required daily, and maintaining this treatment for 6 months or 1 year would be undesirable from both the animal welfare and health management perspectives. Genetic approaches targeting BMP signaling components may be required to clarify its role during chronic disease progression. Finally, several mechanistic relationships proposed in Fig. 8, including the regulation of Runx2/Col10a1 expression, osteoclastogenesis through the sclerostin-RANKL/OPG axis, and macrophage polarization, were inferred from the combination of the present findings and previous literature. Direct causal validation of these pathways will require future cell type-specific and genetic studies.

In conclusion, we have demonstrated that canonical BMP–Smad1/5 signaling was broadly activated in articular cartilage, subchondral bone, and synovium in the mCTA model, and that pharmacological inhibition of this pathway partially attenuated cartilage hypertrophy and degeneration, subchondral bone resorption, and synovial inflammation with pro-inflammatory macrophage polarization. These findings suggest that BMP–Smad1/5 signaling may represent a potential therapeutic target for CTA and warrant further investigation of pathway modulation as a disease-modifying approach.

CRediT authorship contribution statement

Conception and design of the study: T. Iuchi, S. M. Collection and assembly of data: T. Iuchi, K. S., T. Ide, S. T., S. S., K. U. Analysis and interpretation of data: T. Iuchi, K. S., T. Ide, S. T., S. S., K. U., Y. M., H. Tawaratsumida, T. Ijuin, S. M. Drafting of the article: S. M., T. Iuchi. Critical revision of the article: T. Iuchi, K. S., S. M., N. T. Statistical expertise: S. T., H. Tominaga. Acquisition of funding: S. M., H. Tominaga, N. T. Final approval of the article: all authors. All authors take responsibility for the integrity of the work as a whole, from inception to the finished article.

Data availability

The data supporting the findings of this study are available upon request. The single-cell RNA sequencing data generated in this study have been deposited in the NCBI Gene Expression Omnibus under accession number GSE341138.

Declaration of generative AI and AI-assisted technologies in the writing process

During the preparation of this work the authors used ChatGPT to refine the English expressions used in the writing of this paper. After using this tool, the authors reviewed and edited the text as needed and take full responsibility for the content of the article.

Role of the funding source

The study was supported by Japan Society for the Promotion of Science Grants-in-Aid for Scientific Research (C) (contract nos. 22K09336, 22K09309, 24K12333, and 25K12462). The funding source had no role in the study design; collection, analysis, or interpretation of data; the writing of the manuscript; or the decision to submit the manuscript.

Conflict of interest

There are no conflicts of interest to declare.

Acknowledgments

We are grateful to Hui Gao and Miki Sakoda for providing technical assistance. We also thank Mark Cleasby, PhD, from Edanz (https://jp.edanz.com/ac) for editing a draft of this manuscript.

Appendix A. Supplementary data

Supplementary data to this article can be found online at https://doi.org/10.1016/j.ocarto.2026.100884.

References

[1] A. Hasegawa, T. Mihata, K. Fukunishi, A. Uchida, M. Neo, Relationship between the Hamada grade and underlying pathological conditions in the rotator cuff and long head of biceps in symptomatic patients with rotator cuff tears, JSES Int. 6 (2022) 488–494, https://doi.org/10.1016/j.jseint.2022.01.012.

[2] T. Mihata, T.Q. Lee, C. Watanabe, K. Fukunishi, M. Ohue, T. Tsujimura, et al., Clinical results of arthroscopic superior capsule reconstruction for irreparable rotator cuff tears, Arthroscopy 29 (2013) 459–470, https://doi.org/10.1016/j.arthro.2012.10.022.

[3] C.S. Neer 2nd, E.V. Craig, H. Fukuda, Cuff-tear arthropathy, J Bone Joint Surg Am 65 (1983) 1232–1244.

[4] M. Elsharkawi, B. Cakir, H. Reichel, T. Kappe, Reliability of radiologic glenohumeral osteoarthritis classifications, J. Shoulder Elb. Surg. 22 (2013) 1063–1067, https://doi.org/10.1016/j.jse.2012.11.007.

[5] K. Hamada, K. Yamanaka, Y. Uchiyama, T. Mikasa, M. Mikasa, A radiographic classification of massive rotator cuff tear arthritis, Clin. Orthop. Relat. Res. 469 (2011) 2452–2460, https://doi.org/10.1007/s11999-011-1896-9.

[6] H. Tawaratsumida, T. Iuchi, Y. Masuda, T. Ide, S. Maesako, T. Miyazaki, et al., Zoledronate alleviates subchondral bone collapse and articular cartilage degeneration in a rat model of rotator cuff tear arthropathy, Osteoarthr. Cartil. 33 (2025) 101–115, https://doi.org/10.1016/j.joca.2024.08.005.

[7] T. Ijuin, T. Iuchi, H. Tawaratsumida, Y. Masuda, A. Tokushige, S. Maeda, et al., Development of a novel animal model of rotator cuff tear arthropathy replicating clinical features of progressive osteoarthritis with subchondral bone collapse, Osteoarthr Cartil Open 5 (2023) 100389, https://doi.org/10.1016/j.ocarto.2023.100389.

[8] N. Kamiya, Y. Mishina, New insights on the roles of BMP signaling in bone-A review of recent mouse genetic studies, Biofactors 37 (2011) 75–82, https://doi.org/10.1002/biof.139.

[9] A. Garcia De Vinuesa, S. Abdelilah-Seyfried, P. Knaus, A. Zwijsen, S. Bailly, BMP signaling in vascular biology and dysfunction, Cytokine Growth Factor Rev. 27 (2016) 65–79, https://doi.org/10.1016/j.cytogfr.2015.12.005.

[10] K. Uekama, T. Iuchi, T. Ide, K. Shimanoe, Y. Masuda, S. Takada, et al., Stepwise loss of shoulder stabilizers induces humeral head migration and progression of cuff tear arthropathy in a rat model, J. Shoulder Elb. Surg. (2026), https://doi.org/10.1016/j.jse.2026.05.036.

[11] S.Y. Chien, C.H. Tsai, S.C. Liu, C.C. Huang, T.H. Lin, Y.Z. Yang, et al., Noggin inhibits IL-1β and BMP-2 expression, and attenuates cartilage degeneration and subchondral bone destruction in experimental osteoarthritis, Cells 9 (2020), https://doi.org/10.3390/cells9040927.

[12] N. Fukui, Y. Zhu, W.J. Maloney, J. Clohisy, L.J. Sandell, Stimulation of BMP-2 expression by pro-inflammatory cytokines IL-1 and TNF-α in normal and osteoarthritic chondrocytes, J Bone Joint Surg Am 85-A (Suppl 3) (2003) 59–66, https://doi.org/10.2106/00004623-200300003-00011.

[13] M.L. Perez-Lozano, L. Sudre, S. Van Eegher, D. Citadelle, A. Pigenet, M.H. Lafage-Proust, et al., Gremlin-1 and BMP-4 overexpressed in osteoarthritis drive an osteochondral-remodeling program in osteoblasts and hypertrophic chondrocytes, Int. J. Mol. Sci. 23 (2022), https://doi.org/10.3390/ijms23042084.

[14] K. Itoh, N. Udagawa, T. Katagiri, S. Iemura, N. Ueno, H. Yasuda, et al., Bone morphogenetic protein 2 stimulates osteoclast differentiation and survival supported by receptor activator of nuclear factor-κB ligand, Endocrinology 142 (2001) 3656–3662, https://doi.org/10.1210/endo.142.8.8300.

[15] E.D. Jensen, L. Pham, C.J. Billington Jr., K. Espe, A.E. Carlson, J.J. Westendorf, et al., Bone morphogenic protein 2 directly enhances differentiation of murine osteoclast precursors, J. Cell. Biochem. 109 (2010) 672–682, https://doi.org/10.1002/jcb.22462.

[16] M. Okamoto, J. Murai, H. Yoshikawa, N. Tsumaki, Bone morphogenetic proteins in bone stimulate osteoclasts and osteoblasts during bone development, J. Bone Miner. Res. 21 (2006) 1022–1033, https://doi.org/10.1359/jbmr.060411.

[17] S. Maesako, T. Tasaki, K. Uekama, S. Yokoyama, S. Maeda, I. Kitazono, et al., Humeral head in rotator cuff tear arthropathy shows reduced cartilage damage and uniform subchondral bone osteoporosis: a histomorphometric analysis, JSES Int. 10 (2026) 101435, https://doi.org/10.1016/j.jseint.2025.101435.

[18] P.M. Van Der Kraan, E.N. Blaney Davidson, W.B. Van Den Berg, Bone morphogenetic proteins and articular cartilage: to serve and protect or a wolf in sheep clothing's? Osteoarthr. Cartil. 18 (2010) 735–741, https://doi.org/10.1016/j.joca.2010.03.001.

[19] A. Scharstuhl, E.L. Vitters, P.M. Van Der Kraan, W.B. Van Den Berg, Reduction of osteophyte formation and synovial thickening by adenoviral overexpression of transforming growth factor β/bone morphogenetic protein inhibitors during experimental osteoarthritis, Arthritis Rheum. 48 (2003) 3442–3451, https://doi.org/10.1002/art.11328.

[20] A.P. Jaswal, B. Kumar, A.J. Roelofs, S.F. Iqbal, A.K. Singh, A.H.K. Riemen, et al., BMP signaling: a significant player and therapeutic target for osteoarthritis, Osteoarthr. Cartil. 31 (2023) 1454–1468, https://doi.org/10.1016/j.joca.2023.05.016.

[21] J. Hao, J.N. Ho, J.A. Lewis, K.A. Karim, R.N. Daniels, P.R. Gentry, et al., In vivo structure-activity relationship study of dorsomorphin analogues identifies selective VEGF and BMP inhibitors, ACS Chem. Biol. 5 (2010) 245–253, https://doi.org/10.1021/cb9002865.

[22] M.D. Neely, M.J. Litt, A.M. Tidball, G.G. Li, A.A. Aboud, C.R. Hopkins, et al., DMH1, a highly selective small molecule BMP inhibitor promotes neurogenesis of hiPSCs: comparison of PAX6 and SOX1 expression during neural induction, ACS Chem. Neurosci. 3 (2012) 482–491, https://doi.org/10.1021/cn300029t.

[23] G. Sanchez-Duffhues, E. Williams, M.J. Goumans, C.H. Heldin, P. Ten Dijke, Bone morphogenetic protein receptors: structure, function and targeting by selective small molecule kinase inhibitors, Bone 138 (2020) 115472, https://doi.org/10.1016/j.bone.2020.115472.

[24] D.W. Engers, A.Y. Frist, C.W. Lindsley, C.C. Hong, C.R. Hopkins, Synthesis and structure-activity relationships of a novel and selective bone morphogenetic protein receptor (BMP) inhibitor derived from the pyrazolo[1.5-a]pyrimidine scaffold of dorsomorphin: the discovery of ML347 as an ALK2 versus ALK3 selective MLPCN probe, Bioorg. Med. Chem. Lett 23 (2013) 3248–3252, https://doi.org/10.1016/j.bmcl.2013.03.113.

[25] H. Pan, N. Fleming, C.C. Hong, Y. Mishina, D.S. Perrien, Methods for the reliable induction of heterotopic ossification in the conditional Alk2(Q207D) mouse, J. Musculoskelet. Neuronal Interact. 20 (2020) 149–159.

[26] A. Zingman, H. Li, L. Sundem, B. Dehority, M. Geary, T. Fussel, et al., Shoulder arthritis secondary to rotator cuff tear: a reproducible murine model and histopathologic scoring system, J. Orthop. Res. 35 (2017) 506–514, https://doi.org/10.1002/jor.23383.

[27] K. Nagira, Y. Ikuta, M. Shinohara, Y. Sanada, T. Omoto, H. Kanaya, et al., Histological scoring system for subchondral bone changes in murine models of joint aging and osteoarthritis, Sci. Rep. 10 (2020) 10077, https://doi.org/10.1038/s41598-020-66979-7.

[28] O. Korchynskyi, P. Ten Dijke, Identification and functional characterization of distinct critically important bone morphogenetic protein-specific response elements in the Id1 promoter, J. Biol. Chem. 277 (2002) 4883–4891, https://doi.org/10.1074/jbc.M111023200.

[29] H. Yasuda, Discovery of the RANKL/RANK/OPG system, J. Bone Miner. Metabol. 39 (2021) 2–11, https://doi.org/10.1007/s00774-020-01175-1.

[30] J. Xiong, M. Onal, R.L. Jilka, R.S. Weinstein, S.C. Manolagas, C.A. O'brien, Matrix-embedded cells control osteoclast formation, Nat. Med. 17 (2011) 1235–1241, https://doi.org/10.1038/nm.2448.

[31] J.A. Abboud, L.J. Soslowsky, Interplay of the static and dynamic restraints in glenohumeral instability, Clin. Orthop. Relat. Res. (2002) 48–57, https://doi.org/10.1097/00003086-200207000-00007.

[32] C.R. Adams, A.M. Demartino, G. Rego, P.J. Denard, S.S. Burkhart, The rotator cuff and the superior capsule: why we need both, Arthroscopy 32 (2016) 2628–2637, https://doi.org/10.1016/j.arthro.2016.08.011.

[33] R.Z. Hsieh, K.C. Huang, Y.P. Su, C.S. Shi, S.F. Chang, The potential role of bone morphogenetic protein-2/-4 in excessive mechanical overloading-initiated joint degeneration, J. Cell. Physiol. 240 (2025) e31509, https://doi.org/10.1002/jcp.31509.

[34] M. Sato, T. Ochi, T. Nakase, S. Hirota, Y. Kitamura, S. Nomura, et al., Mechanical tension-stress induces expression of bone morphogenetic protein (BMP)-2 and BMP-4, but not BMP-6, BMP-7, and GDF-5 mRNA, during distraction osteogenesis, J. Bone Miner. Res. 14 (1999) 1084–1095, https://doi.org/10.1359/jbmr.1999.14.7.1084.

[35] R. Suzuki, E. Nemoto, H. Shimauchi, Cyclic tensile force up-regulates BMP-2 expression through MAP kinase and COX-2/PGE2 signaling pathways in human periodontal ligament cells, Exp. Cell Res. 323 (2014) 232–241, https://doi.org/10.1016/j.yexcr.2014.02.013.

[36] H. Enomoto, M. Enomoto-Iwamoto, M. Iwamoto, S. Nomura, M. Himeno, Y. Kitamura, et al., Cbfa1 is a positive regulatory factor in chondrocyte maturation, J. Biol. Chem. 275 (2000) 8695–8702, https://doi.org/10.1074/jbc.275.12.8695.

[37] Q. Zheng, G. Zhou, R. Morello, Y. Chen, X. Garcia-Rojas, B. Lee, Type X collagen gene regulation by Runx2 contributes directly to its hypertrophic chondrocyte-specific expression in vivo, J. Cell Biol. 162 (2003) 833–842, https://doi.org/10.1083/jcb.200211089.

[38] B. Heubel, A. Nohe, The role of BMP signaling in osteoclast regulation, J. Dev. Biol. 9 (2021), https://doi.org/10.3390/jdb9030024.

[39] C. Liu, Q. Sun, J. Xu, W. Shen, H. Li, L. Yang, The role of bone morphogenetic protein 4 in microglial polarization in the process of neuropathic pain, J. Inflamm. Res. 15 (2022) 2803–2817, https://doi.org/10.2147/JIR.S356531.

[40] B. Hopwood, A. Tsykin, D.M. Findlay, N.L. Fazzalari, Microarray gene expression profiling of osteoarthritic bone suggests altered bone remodelling, WNT and transforming growth factor-β/bone morphogenic protein signalling, Arthritis Res. Ther. 9 (2007) R100, https://doi.org/10.1186/ar2301.

[41] C.H. Chou, C.C. Wu, I.W. Song, H.P. Chuang, L.S. Lu, J.H. Chang, et al., Genome-wide expression profiles of subchondral bone in osteoarthritis, Arthritis Res. Ther. 15 (2013) R190, https://doi.org/10.1186/ar4380.

[42] T. Olah, M. Cucchiarini, H. Madry, Temporal progression of subchondral bone alterations in OA models involving induction of compromised meniscus integrity in mice and rats: a scoping review, Osteoarthr. Cartil. 32 (2024) 1220–1234, https://doi.org/10.1016/j.joca.2024.06.002.

[43] Y. Hu, X. Chen, S. Wang, Y. Jing, J. Su, Subchondral bone microenvironment in osteoarthritis and pain, Bone Res. 9 (2021) 20, https://doi.org/10.1038/s41413-021-00147-z.

[44] E.E. Vaysbrot, M.C. Osani, M.C. Musetti, T.E. Mcalindon, R.R. Bannuru, Are bisphosphonates efficacious in knee osteoarthritis? A meta-analysis of randomized controlled trials, Osteoarthr. Cartil. 26 (2018) 154–164, https://doi.org/10.1016/j.joca.2017.11.013.

[45] L.J. Soslowsky, J.E. Carpenter, C.M. Debano, I. Banerji, M.R. Moalli, Development and use of an animal model for investigations on rotator cuff disease, J. Shoulder Elb. Surg. 5 (1996) 383–392, https://doi.org/10.1016/s1058-2746(96)80070-x.